arXiv:astro-ph/0501484v1 22 Jan 2005

A theoretical look at the direct detection of giant planets outside the Solar System

Adam Burrows

Department of Astronomy, The University of Arizona, Tucson, AZ 85721

e-mail: aburrows@as.arizona.edu

I. HEADING

Astronomy is at times a science of unexpected discovery. When it is, and if we are lucky, new intellectual territories emerge to challenge our views of the cosmos. The recent indirect detections using high-precision Doppler spectroscopy of now more than one hundred giant planets orbiting more than one hundred nearby stars is an example of such rare serendipity. What has been learned has shaken our preconceptions, for none of the planetary systems discovered to date is like our own. However, the key to unlocking a planet's chemical, structural, and evolutionary secrets is the direct detection of the planet's light. I review the embryonic theory of the spectra, atmospheres, and light curves of irradiated giant planets and put this theory into the context of the many proposed astronomical campaigns to image them.

II. INTRODUCTION: THE NEWLY-DISCOVERED WORLDS

Direct detection of an extrasolar planet requires that its dim light be separated from under the glare of its bright parent star. However, such high-contrast imaging (e.g., a part in 10^{7-10} in the visible) has not to date been achieved. Instead, the vast majority of known extrasolar giant planets (EGPs) have been discovered from the ground using the indirect technique of high-precision stellar spectroscopy [1–3]. Due to gravitational attraction, an

orbiting planet induces a Doppler wobble in its parent star. If the planet is massive and close enough, the periodic variation in the stellar spectral lines can be measured. The planet's period (P), eccentricity (e), orbital semi-major axis (a), and projected mass ($M_p \sin(i)$), where i is the inclination of the orbit, can thereby be determined. The larger $M_p \sin(i)$, the larger the signal. This is the reason the first planets detected were the EGPs. Terrestrial planets, such as Earth and Venus, are $\sim$300 times lighter than Jupiter, while ice giants, such as Uranus and Neptune, are $\sim$20 times lighter.

Before I delve into the physical theory of EGPs and their direct detection, I summarize the basic facts of the known members of the EGP family. The first extrasolar giant planet culled was 51 Peg b [1] and it is in a tight 4.2-day orbit, one hundred times closer to its primary than is Jupiter to the Sun. To date, more than 140 EGPs/planets have been discovered, more than 25 of which are in more than 10 multiple systems. 55 Cancri houses a quadruplet [4], one of which has a mass near that of Neptune ($\sim$17 Earth masses), υ And house a triplet, and GJ 876 houses a doublet in a two-to-one orbital resonance. (We follow the convention by which the planet's name is given by the star's name, with an appended lower-case letter, either b, c, or d, in discovery order.)

The projected masses of the known Doppler planets vary from $\sim$0.06 (!) M_J to above 10 M_J, where M_J is a Jupiter mass, which is 318 Earth masses or roughly 10^{-3} solar masses. The more massive objects may be brown dwarfs with a different provenance (see Box). Radial-velocity (Doppler) techniques can not distinguish EGPs and Neptune-mass planets from brown dwarfs. The orbital periods of the known EGPs span a vast range from $\sim$1.2 *days* to $\sim$12 *years*, their semi-major axes extend from $\sim$0.022 AU to $\sim$6.0 AU, where an AU is an Astronomical Unit, the distance between the Earth and the Sun, and their orbital eccentricities vary from 0.0 to above 0.9. For comparison, Jupiter resides 5.2 AU from our Sun, has an orbital period of $\sim$12 years, and has an orbital eccentricity of $\sim$0.05. Table 1 provides these basic data for a representative subset of the current EGP bestiary. The extremely close-in EGPs, such as 51 Peg b, τ Boo b, HD209458b, and OGLE-TR56b [5–7], were a surprise, but no less so than was the heterogeneity of the masses and orbital

properties of the emerging EGP family. To be sure, the Doppler technique selects for the closer representatives, but they must exist to be detected. As would be expected due to tidal dissipation, the close-in EGPs with orbital distances smaller than ∼0.06 AU all have nearly circular orbits.

There seems to be a correlation between the probability of finding an EGP and the metallicity of its parent star. The "metallicity" of a star is the mass fraction of elements, such as carbon, oxygen, nitrogen, neon, magnesium, silicon and iron, that are heavier than helium. Hydrogen and helium predominate in stars and giant planets, comprising ∼98% by mass of the Sun. The more super-solar the heavy-element composition of the potential parent, the more likely we are to find an EGP in orbit. This may be a hint concerning the processes of giant planet formation, and is in keeping with the 3-5×solar excesses measured in Jupiter and Saturn. The current census reveals that there is a ∼5% a priori chance of finding a giant planet by the Doppler technique around a nearby ($\lesssim$ 50 parsecs ≡ 160 light-years) star, but a ∼20% chance of finding one around a star with at least twice the Sun's metallicity (J. Valenti & D.A. Fischer, in preparation).

Presumably, the inclinations of EGP orbits are distributed randomly on the sky. Hence, the probability that the orbit is edge-on ($i = 90°$) is approximately $R_*/(2a)$, where R_* is the stellar radius. Given this, the close-in EGPs have the largest chance of transiting the stellar disk, during which time the star will dim by a fraction $(R_p/R_*)^2$, where R_p is the planet's radius. Since R_J (the radius of Jupiter, $\sim 7.14 \times 10^4$ kilometers) is roughly 10% of the radius of the Sun, this ratio is expected to be roughly 1%. A 1% dimming is easily detectable from the ground. At a=0.045 AU and a distance (d) of 47 parsecs, the planet around the F8V/G0V star HD209458 was the first of only a handful of EGPs that are now known to transit their primaries and a periodic dimming at the ∼1.6% level was measured [8–10]. The transit of HD209458 lasts ∼3 hours (out of a total period of 3.524738 days). This was followed by the photometrically-selected transiting EGPs OGLE-TR-56b, OGLE-TR-113b, OGLE-TR-132b, OGLE-TR-111b, and TrES-1 [5–7,11–13]. Many more EGP transits are anticipated during the *Kepler* [14] and *Corot* [15] space missions. These projects are

focussed on detecting transits around a fraction of the tens of thousands of stars they will monitor and will boast photometric accuracy ($\sim 10^{-5}$) sufficient to measure not only transits by EGPs, but by Earth-like planets. The import of an EGP transit lies in the simultaneous measurement of both the orbital inclination (and, hence, with Doppler spectroscopy, the mass) and the radius of the planet. Knowledge of R_p and M_p (with some knowledge of the star) can be used to constrain theories of the structure and evolution of the close-in EGP [16–18]. Currently, non-transiting EGPs are mute concerning such physical information.

HD209458 is close and bright enough that the STIS instrument on HST was used not only to obtain photometric precision of $\sim$0.01% [10], but to distinguish a difference at the 4-σ level in the planetary transit radius in and out of the Na-D line at 0.589 μm . In this way, neutral sodium atoms were discovered in HD209458b's atmosphere [19–21]. Though indirect, this is the first measurement of the composition of the atmosphere of an extrasolar planet. Since then, the Lyman-α line of hydrogen has similarly been detected in HD209458b's atmosphere [22], and by the large magnitude ($\sim$15%) of the photometric dip at this UV wavelength (λ) a planetary wind [23] comprised of molecular break-up products has been inferred. However interesting, transits are rare and no substitute for direct imaging and optical and infrared spectra. Spectra can provide diagnostics for atmospheric composition, radius, gravity, and mass. Images are ground truth for the existence of a planet and provide orbital information that complements that gleaned from Doppler measurements. Furthermore, direct detection might be able to distinguish the different models of giant planet formation, such as nucleation around an ice/rock core [24] and direct collapse [25], and can probe the outer orbits where the majority of EGPs might reside.

Since the indirect radial-velocity technique for EGP discovery selects for the closer variety, it is likely that a large reservoir of giants exists at distances and orbital periods beyond the reach of Doppler spectroscopy. Furthermore, the best theory for the orbits of the closest EGPs is that they migrated in from further out during the early phase of star and planet formation [26]. This too would imply that a large pool of EGPs resides at larger separations. Indeed, it may be that the majority of stars in the solar neighborhood harbor planetary

systems, that only new techniques can reveal. This is where the direct planet detection methods, most effective at large angular distances from the parent star, will come into their own.

III. THEORETICAL ATMOSPHERES AND CHEMISTRY OF EGPS

After formation, without any significant internal sources of energy, an EGP gradually cools and shrinks. Its rate of cooling can be moderated by stellar irradiation, or by hydrogen/helium phase separation when old and light [27], but is inexorable. Jupiter itself is still cooling and its total infrared plus optical luminosity is about twice the power intercepted from the Sun. The rate of cooling is a function of mass and composition, with more massive EGPs cooling more slowly. Hence, the instantaneous state of an EGP is a function of mass, age, composition, orbital distance, and stellar type, not just mass and composition.

Unlike a star, EGP atmospheric temperatures are sufficiently low that chemistry is destiny. This is a distinguishing characteristic of substellar-mass objects (SMOs). The atmosphere of a gaseous giant planet is the thin outer skin of molecules that regulates its emission spectrum and cooling rate. Molecular hydrogen (H_2) is the overwhelming constituent, followed by atomic helium. An EGP's effective temperature ($T_{\rm eff}$, the temperature of its "photosphere") can vary from ∼1500 K for the more massive EGPs at birth to ∼50 K for the least massive EGPs after a Hubble time. This wide range translates into a rich variety of atmospheric constituents that for a given mass and elemental composition evolves significantly. At birth, Jupiter had a $T_{\rm eff}$ near 600-1000 K and the appearance of a T dwarf [28] brown dwarf. It had no ammonia or water clouds and, due to the presence of atomic sodium in its hot atmosphere, had a magenta color in the optical [29]. Its atmosphere was depleted of aluminum, silicon, iron, calcium, and magnesium due to the formation and settling to depth of the refractory silicates ("dirt") that condense in the temperaure range ∼1700-2500 K [30–32]. Water vapor (steam) was the major reservoir of oxygen, gaseous methane was the major reservoir of carbon, gaseous ammonia and molecular nitrogen were

the reservoirs of nitrogen, and H_2S was the reservoir of sulfur. As it cooled, the layer of alkali metals was buried below the photosphere to higher pressures, but gaseous H_2, H_2O, NH_3, and CH_4 persisted to dominate the atmospheric composition. At a T_{eff} of ∼400 K, water condensed in the upper atmosphere and water clouds appeared. This occurred within its first 100 million years. Within less than a gigayear, when T_{eff} reached ∼160 K, ammonia clouds appeared on top of the water clouds, and this layering persists to this day. Stellar irradiation retards cloud formation, as does a large EGP mass, which keeps the EGP hot longer. Around a G2V star like the Sun, at 5 Gyr and for an EGP mass of 1.0 M_J , water clouds form at 1.5 AU, whereas ammonia clouds form beyond 4.5 AU [33]. Jupiter's and Saturn's current effective temperatures are 124.4 K and 95 K, respectively. Jupiter's orbital distance and age are 5.2 AU and 4.6 Gyr. The orbital distance, mass, and radius of a coeval Saturn are 9.5 AU, 0.3 M_J , and 0.85 R_J . However, as an EGP of whatever mass cools, its atmospheric composition evolves through a similar chemical and condensation sequence. Figure 1 depicts the atmospheric temperature/pressure (T/P) profile for a sequence of 1-M_J , 5-Gyr models as a function of orbital distance from a G2V star. As the planet "moves" outward, its atmospheric temperature at a given pressure decreases. Superposed on the plot are the H_2O and NH_3 condensation lines. In an approximate sense, a given atmospheric composition and temperature can result from many combinations of orbital distance, planet mass, stellar type, and age. This lends an added degree of complexity to the study of EGPs with which the study of stars does not need to wrestle.

The atmospheres of close-in EGPs ("roasters") at orbital distances of ∼0.02-0.07 AU from a G, F, or K star are heated and maintained at temperatures of 1000-2000 K, roughly independent of planet mass or composition. An edge star of the solar-composition, hydrogen-burning main sequence (M_*∼75 M_J) has a T_{eff} of ∼1700 K. Therefore, an irradiated EGP, with a radius comparable to that of such a star, can be as luminous. Its atmospheric composition is predominantly H_2, He, H_2O, Na, K, and CO. At high temperatures, carbon is generally in carbon monoxide. This is the dominant molecule of carbon for M dwarfs with T_{eff}s of 2200-3500 K. At the highest T_{eff}s, clouds of iron particulates can form and

persist in the upper atmosphere, as may be the case in HD209458b. There are, however, significant day/night differences and unique reflective properties that distinguish a roaster from a lone and isolated edge star. Exotic general circulation models (GCMs) [34–36] may soon be necessary to understand the equatorial currents, jet streams, day/night differences, terminator chemistry, and global wind dynamics of severely irradiated roasters, in particular, and of orbiting, rotating EGPs, in general.

It is useful to note that a young EGP in a wide orbit with a mass of 1.0 to 5.0 M_J has an atmosphere and spectrum that are similar to those of an old brown dwarf with a mass of 30-60 M_J . As it evolves, the spectroscopic class of a giant planet can transition from that of a hot M dwarf, into an L dwarf (where the silicate clouds are *in* the atmosphere), then into a T dwarf, ending up in the territory, as yet unexplored, between the Jovian planets and the "stars." If its mass is low enough, an EGP can cool within gigayears to assume the aspect of our Jovian planets. Hence, by chemistry, clouds, and T_{eff}, the study of brown dwarfs and EGPs are inextricably linked.

Finally, the best theoretical fits to Saturn's internal structure suggest that it contains a 5–20 Earth-mass core of heavy elements [37]. This core of (perhaps) ice and rock may have been the nucleus around which Saturn formed and resembles the ice giants Neptune and Uranus. The latter may be aborted giant planets that were able to accrete but little hydrogen from the protosolar/protoplanetary nebula. The Neptune-mass extrasolar planet, 55 Cancri e, may be a stripped or aborted EGP. An alternative mode of giant planet formation is by direct collapse [25]. Under such a scenario, one would expect a closer correspondence between the heavy-element abundances of planet and parent star. Hence, the composition of its atmosphere and its heavy-element-dependent radius might be keys to an EGP's formation. These are in principle measureable.

Box: Brown Dwarfs

Brown dwarfs are substellar-mass objects (SMOs) ($\lesssim$ 0.07 solar masses $\equiv\sim$75

M_J) that are unable to ignite light hydrogen stably to become a star, but are otherwise formed like stars. The radiative surface losses of a star balance the thermonuclear power generated in its core. This requires sufficient mass. The surface losses of a less-massive brown dwarf are not fully compensated by thermonuclear burning and it cools inexoribly after formation over a Hubble time. Nevertheless, brown dwarfs constitute the low-mass, low-temperature extension of the stellar family and are an important subject in their own right [29,38]. Masses in the range of $\sim$10 M_J to $\sim$75 M_J are frequently discussed, but overlap with the mass distribution of the EGP family is entirely possible.

IV. SPECTRAL FEATURES OF EGPS

In principle, as with stellar atmospheres, direct detection of the spectrum of an extrasolar giant planet can reveal its elemental composition, radius, gravity ($GM_p/{R_p}^2$), and T_{eff}. Furthermore, when a cloud dwells in its atmosphere, its associated absorption and scattering properties might be used to determine the cloud's particle size and makeup. Moreover, short-term temporal variations of the planet's flux and spectrum might indicate rotation and/or meteorology. Finally, irradiation introduces the star-planet-Earth angle as an important parameter, so the orbit's orientation and instantaneous orbital phase must be factored in (§V). Along with the dependences on M_p, age, stellar type, and orbital distance, this variety of influences and parameters makes the study of EGP spectral signatures and light curves, and their inversion to obtain planetary properties, rather complicated.

Nevertheless, the molecular mix described in §III determines the emergent and reflected spectrum. Though H_2 is abundant, it has no permanent electric dipole moment, and, hence, a very low photon absorption cross section in the optical and infrared. Similarly, helium is all but transparent. The result is that gaseous water vapor, with its strong absorption features from 0.94 μm to $\sim$7 μm , can define much of an EGP's spectrum. Because water

resides in both the Earth's and an EGP's atmosphere, the water bands that bracket and determine the Earth's photometric windows at $\sim$1.0 μm (Z), $\sim$1.25 μm (J), $\sim$1.65 μm (H), $\sim$2.2 μm (K), $\sim$3.45 μm (L'), and $\sim$4-5 μm (M), through which ground-based infrared astronomy is possible, are exactly the same windows in an EGP or brown dwarf atmosphere through which emergent flux can pour. Thus, and fortuitously for brown dwarf observations, the emission peaks for SMOs coincide with the classic Terrestrial atmospheric bandpasses.

In lieu of measurements, theory fills the vacuum. Figure 2, taken from Burrows, Sudarsky, & Hubeny [33], depicts "phase-averaged" [39] planet/star flux ratios (f) from 0.5 μm to 30 μm for a 1-M_J/5-Gyr EGP in a circular orbit at various distances from a G2V star like the Sun. These models are the same as those depicted in Fig. 1. Similar plots for different assumed parameters can be generated. The water absorption troughs are manifest throughout. For the closer EGPs at higher atmospheric temperatures, carbon resides in CO and methane features are weak. For these close-in EGPs, the Na-D line at 0.589 μm and the corresponding resonance line of K I at 0.77 μm are important absorbers, suppressing flux in the visible bands. Otherwise, the optical flux is buoyed by Rayleigh scattering of stellar light. As a increases, methane forms and the methane absorption features in the optical (most of the undulations seen in Fig. 2 for $a \gtrsim 0.5$ AU shortward of 1 μm), at $\sim$3.3 μm, and at $\sim$7.8 μm appear. Concomitantly, Na and K disappear from the atmosphere and the fluxes from $\sim$1.5 μm to $\sim$4 μm drop. For all models, the mid-infrared fluxes longward of $\sim$4 μm are due to self-emission, not reflection. As Fig. 2 makes clear, for larger orbital distances a bifurcation between a reflection component in the optical and an emission component in the mid-infrared appears. This separation into components is not so straightforward for the closer, more massive, or younger family members. For these EGPs, either the large residual heat coming from the core or the severe insolation prop up the fluxes from 1 to 4 μm. The more massive EGPs, or, for a given mass, the younger EGPs, have larger J, H, and K band fluxes. As a result, these bands are diagnostic of mass and age. For EGPs with large orbital distances, the wavelength range from 1.5 μm to 4 μm between the reflection and emission components may be the least favorable search space, unless the SMO is massive or young.

When water or ammonia clouds form, scattering off them enhances the optical fluxes, while absorption by them suppresses fluxes at longer wavelengths in, for example, the 4–5 μm window. Because water and ammonia clouds form in the middle of this distance sequence, the reflection efficiency (or "albedo"; §V) is not a monotonic function of a. These effects are incorporated into Fig. 2, but their precise magnitude depends upon unknown cloud particle size, composition, and patchiness. As a consequence, direct spectral measurements might constrain cloud properties.

Importantly, trace non-equilibrium molecular species, difficult to model, can be present in quantities sufficient to alter colors. Such a "chromophore," whose molecular nature is not yet known, absorbs in the blue and creates the reddish cast of both Jupiter and Saturn, lowering their albedos shortward of 0.55 μm by a factor of $\sim$1.5–2. (Chromophores were not modelled to produce Fig. 2.)

As Fig. 2 suggests, the planet/star contrast ratio is better in the mid- to far-infrared, particularly at wide separations. For such separations, the contrast ratio in the optical can sink to 10^{-10}. For the closest-in EGPs, such as HD209458b, OGLE-TR56b, 51 Peg b, and τ Boo b, the contrast ratio in the optical is between 10^{-5} and 10^{-6} and is more favorable. Such EGPs are not shown in Fig. 2; there are in fact about 20 known EGPs with orbital distances less than 0.08 AU. Due to the possible formation of iron clouds in their atmospheres, HD209458b and OGLE-TR56b may be brighter in the optical than 51 Peg b and may have higher reflection albedos. Figure 3 portrays a generic absolute flux spectrum at 10 parsecs of a close-in EGP ("Class V" in the nomenclature of Sudarsky et al. [39]), not unlike HD209458b. Highlighted are the positions of some of the important spectral features. Since modern telescopes can easily detect fluxes at the milliJansky level, Fig. 3 demonstrates that the fluxes themselves are not small. The problem is seeing the planet from under the glare of the star (§VI). At 10 parsecs and an orbital separation of 0.05 AU, the maximum angular separation is a challenging $\sim$5 milliarcsecs.

V. PHASE FUNCTIONS FOR EGPS AND ORBITAL ORIENTATION

The planetary albedo and the phases executed as planets traverse their orbits are central quantities in the theory of EGP light curves. In addition, as we discuss in this section, the wavelength-dependent albedos are strong functions of orbital distance as well. Furthermore, the changing orientation of the illuminated face of a planet from the Earth's perspective translates into a light curve that can show significant flux and color variations. In Fig. 2, these variations were averaged out over the orbit, assumed circular. The longitude independence of Jupiter's T/P profile results in little day/night variation in the mid-infrared and, hence, little phase variation, but such a planet is too cold to be self-luminous enough in the optical for its reflected component not to dominate at these shorter wavelengths. Hence, Jupiter's optical fluxes can vary from superior conjunction (full face) to first quarter (90° from superior conjunction, not seen from Earth) or last quarter (270° from superior conjunction, also not seen from Earth) by a factor of $\sim$3 [40]. Note that the phase dependence of an EGP's light curve in the mid-infrared will depend on the degree to which heat can be efficiently redistributed over its entire face. This will depend on 3-dimensional GCM effects that have not been worked out. For the close-in EGPs, due to expected day/night temperature differences [41,42], it is likely that there will be phase variations at all wavelengths. In particular, phase variations at thermal wavelengths are likely to shed light on the atmospheric dynamics and longitudinal temperature distribution of an EGP.

Since its orbit and orientation play such an important role in an EGP's flux at the Earth and in its interpretation, we summarize the basic formulae and concepts. We restrict ourselves to the optical, for which the concept of an albedo has a clear meaning, but note that the approach we summarize has general applicability.

The planet/star flux ratio (f) is given by:

$$f = p(\mathrm{R_p}/R)^2\Phi(\alpha), \tag{1}$$

where R is the planet/star distance, p is the geometric albedo, $\Phi(\alpha)$ is the phase function, and α is the star-EGP-Earth angle. $\Phi(\alpha)$ is normalized to be 1.0 at full face, thereby defining

the geometric albedo, and is a decreasing function of α. For so-called "Lambert" reflection in which an incident ray on a planetary patch emerges uniformly over the exit hemisphere, p is 2/3 for purely scattering atmospheres and $\Phi(\alpha)$ is given by the formula:

$$\Phi(\alpha) = \frac{\sin(\alpha) + (\pi - \alpha)\cos(\alpha)}{\pi}\,. \tag{2}$$

However, EGP atmospheres are absorbing and the anisotropy of the single scattering phase function for grains, droplets, or molecules results in non-Lambertian behavior. For instance, back-scattering off cloud particles can introduce an "opposition" effect for which the planet appears "anomalously" bright at small αs. This spike might be a useful signature of cloud particle size. Moreover, the light scattered from EGPs is likely to be strongly polarized [43]. The degree of polarization as a function of wavelength and phase angle α can also be used to determine cloud properties. However, polarization will be rather more difficult to measure.

Both p and $\Phi(\alpha)$ are functions of wavelength, but the wavelength-dependence of p is the most severe. In fact, for cloud-free atmospheres, due to strong absorption by molecular bands, p can be as low as 0.03. Rayleigh scattering serves to support p, but mostly in the blue and UV, where, however, chromophores can decrease it. The presence of clouds increases p significantly. For instance, at 0.48 μm , Jupiter's geometric albedo is $\sim$0.46 and Saturn's is 0.39 [44]. Note that for orbital distances less than 1.5 AU, we expect the atmospheres of most EGPs to be clear. The albedo would be correspondingly low. As a consequence, the theoretical albedo is very non-monotonic with distance, ranging in the visible from perhaps $\sim$0.3 at 0.05 AU, to $\sim$0.05 at 0.2 AU, to $\sim$0.4 at 4 AU, to $\sim$0.7 at 15 AU [33,39,45]. In the visible ($\sim$0.55 μm), the geometric albedo for a roaster is severely suppressed by Na-D at 0.589 μm . Due to a methane feature, the geometric albedo can vary from 0.05 at $\sim$0.6 μm to $\sim$0.4 at 0.625 μm . Hence, variations with wavelength and with orbital distance by factors of 2 to 10 are not unexpected. Those planning programs of direct detection should be aware of such possibilities.

$\Phi(\alpha)$ and p must be calculated or measured, but the sole dependence of $\Phi(\alpha)$ on α belies the complications introduced by an orbit's inclination angle (i), eccentricity (e), argument

of periastron (ω), and longitude of ascending node (Ω). Along with the period (P) and an arbitrary zero of time, these are the so-called Keplerian elements of an orbit. Figure 4 diagrams and defines these orientational and orbital parameters. In the plane of the orbit, the angle between the planet and the periastron/periapse (distance of closest approach to the star) at the star is θ. In the jargon of celestial mechanics, θ is the so-called "true anomaly." For an edge-on orbit ($i = 90°$), and one for which the line of nodes is perpendicular to the line of sight ($\Omega = 90°$) and parallel to the star-periapse line ($\omega = 0°$), θ is complementary to α ($\alpha = 90° - \theta$). As a result, $\theta = 0°$ at $\alpha = 90°$ (greatest elongation) and increases with time. Also, for such an edge-on orbit, $\alpha = 0°$ at superior conjunction. In general,

$$\cos(\alpha) = \sin(\theta + \omega)\sin(i)\sin(\Omega) - \cos(\Omega)\cos(\theta + \omega)\,. \tag{3}$$

This is merely an application of the law of cosines.

For a circular orbit, R is equal to the semi-major axis (a). However, a planet in an eccentric orbit can experience significant variation in R, and, therefore, stellar insolation (by a factor of $(\frac{1+e}{1-e})^2$). For example, if $e = 0.3$, the stellar flux varies by $\sim$3.5 along its orbit. For $e = 0.6$, this variation is a factor of 16! Such eccentricities are by no means rare in the sample of known EGPs (cf. Table 1). Therefore, it is possible for the composition of an EGP atmosphere to change significantly during its orbit, for clouds to appear and disappear, and for there to be delays ("hysteresis") in the accommodation of a planet's atmosphere to a varying "insolation" regime. Ignoring the latter, eqs. 1 and 3 can be combined with $\Phi(\alpha)$ and the standard Keplerian formula connecting θ and time for an orbit with a given P and e to derive an EGP's light curve as a function of wavelength, i, e, Ω, ω, and time. The upshot is that, depending upon orientation and eccentricity, the brightness of an EGP can vary in its orbit not at all (for a face-on EGP in a circular orbit) or quite dramatically (e.g., for highly eccentric orbits at high inclination angles). Since astrometric measurements of stellar wobble induced by EGPs can yield the entire orbit (including inclination), data from the Space Interferometry Mission (SIM) [46] (expected to achieve 1-microarcsecond narrow-angle accuracy) or Gaia [47] could provide important supplementary data to aid in

the interpretation of direct detections of EGPs.

As Saturn itself demonstrates, depending upon orbital orientation, planetary rings can greatly augment reflected light [40,48]. Their possible presence is a wild card in the interpretation of direct EGP signatures. Also, since $\Phi(\alpha)$ is wavelength-dependent, the potentially large variation in reflected optical flux with epoch will be complemented by an interesting variation in color. The phase functions $\Phi(\alpha)$ are wavelength-dependent. For example, planets should execute trajectories in the color-color space $V - R$ vs. $B - V$, where B, V, and R are the standard blue, visible, and red bands. These trajectories will be functions of cloud particle size, among other things, and will be useful atmospheric diagnostics. Similar behavior in the near- and mid-infrared colors, though more modest, may be seen.

VI. GROUND-BASED AND SPACE-BASED TELESCOPES FOR DIRECT DETECTION

As Fig. 2 implies, the wide range of planet/star contrast ratios and spectral diagnostics suggests different technological solutions to direct detection. Furthermore, the relative merits of searching in the optical, near-infrared, or the mid-infrared have yet to be determined. Both ground-based (less expensive) and space-based (more capable) paths are being pursued and while a discussion that does justice to the many initiatives whose goal is the remote sensing of EGPs is far beyond the scope of this review, we summarize a few representative approaches.

EGPs, especially if they are young, massive, and close, are bright enough that current 8- to 10-meter class ground-based telescopes or near-term space telescopes (such as the James Webb Space Telescope (JWST) [49] with a 6-meter aperture) might be sensitive enough to pick up their light. This is particularly true in the near- and mid-infrared (see Figs. 2 and 3). However, under the extreme glare of its parent star and at small angular separations of from ∼milliarcsecs to around an arcsecond (Table 1), traditional telescope optics spills far too much light in the vicinity of the planet. The major culprits on the ground are the

turbulence of the atmosphere ("seeing" and scintillation), scattering off dust and the spider mount of the secondary, and imperfections in the mirror(s). Also at issue is the stability of the optical system. Even for perfect optics, the diffraction pattern due to the finite telescope aperture leaves a characteristic "Airy" pattern that for a "Jupiter" at 10 parsecs around a solar-type star would in the optical be hundreds of times brighter.

Hence, for large (8–10-meter) ground-based telescopes, (e.g., the two Kecks [50,51], the four VLTs [52,53], the two Geminis [54], Subaru [55], the binocular LBT [56,57]) and mammoth proposed telescopes (e.g., the 100-meter OWL [58], the 20-meter GMT [59], the 30-meter GSMT [60]), special efforts will be required. These include adaptive optics (AO) to compensate for atmospheric fluctuations (and mirror imperfections) with many hundreds or thousands of fast (millisecond) actuators and very accurate wavefront sensing. The latter can, in principle, be achieved using artificial laser guide stars or stars in the field of view. (With AO, there is usually a bright star close enough to obviate the need for an artificial beacon.) Interferometry to null out the stellar light is also being pursued by the LBT, VLT, and Keck, and the depth of the null is crucial, as is the angular region over which a sufficient null can be achieved. Finally, apodizing masks and/or coronagraphic spots to occult the star and, by diffractive interference, redistribute the star's light away from the planet are highly desirable (and may be necessary). Note that since Dome C in Antartica has some of the best seeing on the planet and the quietest atmosphere, placing a giant next-generation telescope there may have its advantages [61].

An EGP imaging system will be judged by the planet/star contrast ratio, f, it can achieve at a given wavelength and for a given angular separation from the star. Angles of 0.05 to 2.0 arcsecs are contemplated (Table 1), with the requisite contrasts at smaller angles deemed too difficult for first-generation imaging. Note that the actual requirements are a function of distance to the star. As Fig. 2 indicates for a 5-Gyr/1-M_J EGP at 10 parsecs, fs better than 10^{-4} at 10 μm and better than 10^{-8} in the optical might be necessary. At the 4-5 μm bump, fs from 10^{-5} to 10^{-8} may be called for. Fortunately, these performance goals can be relaxed for more massive and younger EGPs at angular separations greater than

$\sim 0.1''$. For the roasters, almost independent of mass and age, f reaches 10^{-3} in the mid-infrared and $\lesssim 10^{-5}$ in the optical, but at the corresponding milliarcsecond separations even these contrast ratios may be too challenging for imaging. Figure 5 compares the theoretically required contrast ratios for the fiducial 5-Gyr/1-M_J EGP at various wavelengths (taken from Fig. 2) as a function of angular separation from a solar-type star at 10 parsecs with the putative capabilities of a sample of proposed imaging systems, both on the ground and in space. Contrast ratios for a 0.5-Gyr/7-M_J EGP in the H band are also shown. Orbit and orientation effects have been ignored and large error bars should be assigned to both theory and projected capability. In addition, care should be taken to compare theoretical numbers with experimental hopes for the same wavebands. In the interests of brevity, we have included multiple wavebands on Fig. 5.

Telescopes are stages of components (primary mirror, secondary mirror, lens, apertures, apodizing masks, coronagraphs, etc.) that in series act on the incident source wavefront to focus light of a desired character on instruments. Daisy-chained together, each "optical" component convolves itself with an input wavefront to produce an output wavefront. In spatial frequency space, the operation of each stage along the optical path is to multiply the Fourier transform of the incident wavefront by a Fourier transform characteristic of that component's optical properties and geometry. If you can introduce components in the optical path that filter or alter the frequency distribution of the wavefront in such a way that its inverse (the spatial distribution of the light in the last image plane) has little or no light in a 2-dimensional angular realm around the star where a planet might reside, then you have a planet-imaging system. Though a telescope's classical angular resolution ($\sim \lambda/D$, where D is the diameter of the telescope primary) improves with decreasing λ, the negative effects of the atmosphere actually diminish with increasing λ. As a result, many ground-based planet-finding initiatives (e.g., MMT(AO) [57], LBT-I, VLT-I, VLT-PF, Keck-I, Gemini-XAOPI/ExAOC, OWL) are planning to optimize in the near- or mid-infrared. Figure 5 summarizes the performance goals of some of them.

In coronagraphic mode, the space-bourne JWST may achieve fs of 10^{-5} to 10^{-6} for

wavelengths from $\sim$1.0 μm to $\sim$5.0 μm. HST/NICMOS has already achieved comparable fs in H band at angular separations from 0.3″ to 1.0″ [62]. However, for single space telescopes without the atmosphere with which to contend, the optical is clearly preferred (small λ/D). Curiously, above the atmosphere mirror imperfections and thermal flexure are still problems and an AO system is necessary to cancel the wavefront errors introduced by the corrugations that remain on an otherwise almost perfect mirror surface after state-of-the-art machining and polishing. Two major space-based projects to image EGPs are being proposed. The first, *EPIC* [63], is a nulling coronagraph which converts a single telescope pupil into a multi-beam nulling interferometer, producing a null which is then filtered by an array of single-mode fibers to suppress the residual scattered light. The design goal of *EPIC* is for fs of 10^{-9} to 10^{-10}. The second, *ECLIPSE* [64,65], is an off-axis coronagraph with an exquisitely-figured 1.8-meter primary that is designed to achieve fs in the V band better than 10^{-9} for angular separations from $\sim$0.1″ to $\sim$2.0″. Both *ECLIPSE* and *EPIC* will be challenging, but if successful will directly detect within $\sim$7 years many EGPs in the solar neighborhood out to 10–15 parsecs.

However, the flagship of the NASA *Origins* program, the Terrestrial Planet Finder (TPF [66]), whose goal is to image planetary systems and extrasolar Earths and to obtain low-resolution ($\lambda/\Delta\lambda$ = 10-20) spectra that may reveal in rudimentary fashion the O_2, H_2O, CH_4, O_3, or CO_2 signatures of life, will also be a formidable instrument for directly detecting and characterizing EGPs. As Fig. 5 indicates, for angular separations between $\sim$0.05″ and $\sim$2.0″, either the more-straightforward optical coronagraphic design (TPF-C) or the multi-telescope infrared (5–20 μm) interferometer (TPF-I/Darwin) would detect EGPs much more readily than the extrasolar Earths that are its primary targets.

For the close-in EGPs, direct imaging seems out of the question for the forseeable future. However, this does not mean that the planetary flux can not be measured. From the ground, there are a variety of techniques to use the planet-plus-star light to distinguish the planetary component (particularly for known roasters). These include 1) using precision photometry to a part in 10^5 (!) to measure the phase variations of the summed optical or near-infrared light,

2) measuring the motion of the light centroid, perhaps best done in the mid-infrared with an Antarctic 30-meter telescope, 3) spectral deconvolution of a known EGP/star system using its RV-measured velocities and ephemeris, and 4) multi-frequency differential interferometric imaging (pioneered for Keck, among others). Further transit studies of HD209458b (such as led to the discovery of the Na-D and Lyman-α features) are certainly warranted. The ground-based methods will be challenging, but less expensive than space-based efforts. However, there is currently in space a micro-satellite, MOST [67], with a 15-centimeter aperture, that is designed to achieve photometric accuracy in the optical of a few$\times 10^{-6}$. It has on its current observing manifest programs to stare at 51 Peg b, τ Boo b, and HD209458b. There have as yet been no announcements.

VII. THE FUTURE

With many programs of direct planet detection planned on a large subset of the LBT, VLT, Keck, Gemini, GMT, GSMT/CELT, and OWL on the ground and HST, *Corot*, *Kepler*, MOST, SIM, Gaia, TPF-C, TPF-I/Darwin, *ECLIPSE*, EPIC, and JWST in space, during the next twenty years there will be an increasing crescendo of new results on extrasolar planets that will completely transform our view of the nature of planetary systems.

EGPs, being brighter, are the natural technological and scientific stepping stones on the path to imaging extrasolar Earths. We will encounter them first. Both the NASA and ESA roadmaps [68] have given planet detection pride of place. Strategies are now being formulated to establish a logical sequence of missions and telescope construction that will optimize the pace of discovery. Moreover, theoretical work in support of mission planning is maturing to the point that it may be ready to interpret what we observe. However, a theorist's prejudices aside, one can't help but wonder: What is it we will actually find? What discoveries will be made? As the hunt for worlds beyond our solar system quickens, an ancient curiosity stirs to ask: What will *our* generation see from that fabled peak in Darien [69]?

REFERENCES

[1] Mayor, M. & Queloz, D. A Jupiter-Mass Companion to a Solar-Type Star. *Nature* **378**, 355 (1995).

[2] Marcy, G.W. and R.P. Butler, R.P. A Planetary Companion to 70 Virginis. *Astrophys. J.* **464**, L147-151 (1996).

[3] see J. Schneider's Extrasolar Planet Encyclopaedia at `http://www.obspm.fr/encycl/encycl.html` for an up-to-date listing.

[4] MacArthur, B. et al. Detection of a Neptune-mass planet in the ρ^1 Cancri system using the Hobby-Eberly Telescope. (55 Cancri e) submitted to *Astrophys. J.* (2004).

[5] Konacki, M., Torres, G., Jha, S., and Sasselov, D. An extrasolar planet that transits the disk of its parent star. *Nature* **421**, 507-509 (2003).

[6] Torres, G, Konacki, M., Sasselov, D., & Jha, S. New Data and Improved Parameters for the Extrasolar Transiting Planet OGLE-TR-56b. *Astrophys. J.* **609**, 1071-1075 (2003).

[7] Sasselov, D. The New Transiting Planet OGLE-TR-56b: Orbit and Atmosphere. *Astrophys. J.* **596**, 1327-1331 (2003).

[8] Henry, G., Marcy, G.W., Butler, R.P., & Vogt, S.S. A Transiting "51 Peg-like" Planet. *Astrophys. J.* **529**, L41-44 (2000).

[9] Charbonneau, D., Brown, T.M., Latham, D.W., & Mayor, M. Detection of Planetary Transits Across a Sun-like Star. *Astrophys. J. Letters* **529**, L45-48 (2000).

[10] Brown, T. M., Charbonneau, D., Gilliland, R.L., Noyes, R.W., and Burrows, A. Hubble Space Telescope Time-Series Photometry of the Transiting Planet of HD 209458. *Astrophys. J.* **552**, 699-709 (2001).

[11] Bouchy, F., Pont, F., Santos, F.C., Melo, C., Mayor, M., Queloz, D., & Udry, S. Two

new "very hot Jupiters" among the OGLE transiting candidates. *Astron. Astrophys.* **421**, L13-16 (2004).

[12] Alonso, R. et al. TrES-1: The transiting planet of a bright K0V star. in press (2004).

[13] Pont, F., Bouchy, F., Queloz, D., Santos, N.C., Melo, C., Mayor, M., & Udry, S. The "missing link": A 4-day period transiting exoplanet around OGLE-TR-111. *Astron. Astrophys.* , in press (astro-ph/0408499) (2004).

[14] Koch, D., Borucki, W., Webster, L., Dunham, E., Jenkins, J., Marrion, J., & Reitsema, H. Kepler: a space mission to detect earth-class exoplanets. *SPIE Conference 3356: Space Telescopes and Instruments V*, 599-607 (1998).

[15] Antonello, E. & Ruiz, S.M. The Corot Mission. *Memoria della Societa Astronomica Italiana* **73**, 1241 (2002).

[16] Burrows, A., Sudarsky, D., & Hubbard, W.B. A Theory for the Radius of the Transiting Giant Planet HD 209458b. *Astrophys. J.* **594**, 545-551 (2003).

[17] Burrows, A., Hubeny, I., Hubbard, W.B., & Sudarsky, D. Theoretical Radii of Transiting Giant Planets: The Case of OGLE-TR-56b. *Astrophys. J.* **610**, L53-56 (2004).

[18] Baraffe, I., Chabrier, G., Allard, F., and Hauschildt, P.H. Evolutionary models for cool brown dwarfs and extrasolar giant planets. The case of HD 209458. *Astron. Astrophys.* **402**, 701-712 (2003).

[19] Charbonneau, D., Brown, T.M., Noyes, R.W., & Gilliland, R.L. Detection of an Extrasolar Planet Atmosphere. *Astrophys. J.* **568**, 377-384 (2002).

[20] Seager, S. & Sasselov, D.D. Theoretical Transmission Spectra during Extrasolar Giant Planet Transits. *Astrophys. J.* **537**, 916-921 (2000).

[21] Hubbard, W.B., Fortney, J.F., Lunine, J.I., Burrows, A., Sudarsky, D., & Pinto, P.A. Theory of Extrasolar Giant Planet Transits. *Astrophys. J.* **560**, 413-419 (2001).

[22] Vidal-Madjar, A., des Etangs, A., Desert, J.-M., Ballester, G.E., Ferlet, R., Hebrard, G., & Mayor, M. An extended upper atmosphere around the extrasolar planet HD209458b. *Nature* **422**, 143-146 (2003).

[23] Burrows, A. & Lunine, J.I. Extrasolar Planets - Astronomical Questions of Origin and Survival. *Nature* **378**, p. 333 (1995).

[24] Mizuno, H. Formation of the Giant Planets. *Progress of Theoretical Physics* **64**, 544-557 (1980).

[25] Boss, A.P. Gas Giant Protoplanet Formation: Disk Instability Models with Thermodynamics and Radiative Transfer. *Astrophys. J.* **563**, 367-373 (2001).

[26] Trilling, D., Benz, W., Guillot, T., W.B. Hubbard, W.B., J.I. Lunine, & Burrows, A. Orbital Migration of Giant Planets: Modeling Extrasolar Planets. *Astrophys. J.* **500**, 428-439 (1998).

[27] Fortney, J.J. & Hubbard, W.B. Effects of Helium Phase Separation on the Evolution of Extrasolar Giant Planets. *Astrophys. J.* **608**, 1039-1049 (2004).

[28] Burgasser, A. et al. The Spectra of T Dwarfs. I. Near-Infrared Data and Spectral Classification. *Astrophys. J.* **564**, 421-451 (2002).

[29] Burrows, A., Hubbard, W.B., Lunine, J.I., & Liebert, J. The theory of brown dwarfs and extrasolar giant planets. *Rev. Mod. Phys.* **73**, 719-765 (2001).

[30] Burrows, A. & Sharp, C.M. Chemical Equilibrium Abundances in Brown Dwarf and Extrasolar Giant Planet Atmospheres. *Astrophys. J.* **512**, 843-863 (1999).

[31] Lodders, K. Alkali Element Chemistry in Cool Dwarf Atmospheres. *Astrophys. J.* **519**, 793-801 (1999).

[32] Lodders, K. & Fegley, B. Atmospheric Chemistry in Giant Planets, Brown Dwarfs, and Low-Mass Dwarf Stars. I. Carbon, Nitrogen, and Oxygen. *Icarus* **155**, 393-424 (2002).

[33] Burrows, A., Sudarsky, D., & Hubeny, I. Spectra and Diagnostics for the Direct Detection of Wide-Separation Extrasolar Giant Planets. *Astrophys. J.* **609**, 407-416 (2004).

[34] Menou, K., Cho, J. Y-K., Seager, S. & Hansen, B.M.S. "Weather" Variability of Close-in Extrasolar Giant Planets. *Astrophys. J.* **587**, L113-116 (2003).

[35] Cho, J. Y-K., Menou, K., Hansen, B.M.S., & Seager, S. The Changing Face of the Extrasolar Giant Planet HD 209458b. *Astrophys. J.* **587**, L117-120 (2003).

[36] Burkert, A., Lin, D.N.C., Bodenheimer, P., Jones, C., & Yorke, H. On the Surface Heating of Synchronously-Spinning Short-Period Jovian Planets. astro-ph/0312476 (2004).

[37] Saumon, D. & Guillot, T. Shock Compression of Deuterium and the Interiors of Jupiter and Saturn. *Astrophys. J.* **609**, 1170-1180 (2004).

[38] Burrows, A., Marley, M., Hubbard, W.B., Lunine, J.I., Guillot, T., Saumon, D., Freedman, R., Sudarsky, D., & Sharp, C. A Nongray Theory of Extrasolar Giant Planets and Brown Dwarfs. *Astrophys. J.* **491**, 856-875 (1997).

[39] Sudarsky, D., Burrows, A., & Pinto, P. Albedo and Reflection Spectra of Extrasolar Giant Planets. *Astrophys. J.* **538**, 885-903 (2000).

[40] Dyudina, U.A., Sackett, P.D., Bayliss, D.D.R., Seager, S., Porco, C., Throop, H.B., & Dones, L. Phase light curves for extrasolar Jupiters and Saturns. astro-ph/0406390 (2004).

[41] Guillot, T. & Showman, A.P. Evolution of "51 Pegasus b-like" planets. *Astron. Astrophys.* **385**, 156-165 (2002).

[42] Showman, A.P. & Guillot, T. Atmospheric circulation and tides of "51 Pegasus b-like" planets. *Astron. Astrophys.* **385**, 166-180 (2002).

[43] Seager, S., Whitney, B.A, & Sasselov, D.D. Photometric Light Curves and Polarization of Close-in Extrasolar Giant Planets. *Astrophys. J.* **540**, 504-520 (2000).

[44] Karkoschka, E. Methane, Ammonia, and Temperature Measurements of the Jovian Planets and Titan from CCD-Spectrophotometry. *Icarus* **133**, 134-146 (1999).

[45] Sudarsky, D., Burrows, A., & Hubeny, I. Theoretical Spectra and Atmospheres of Extrasolar Giant Planets. *Astrophys. J.* **588**, 1121-1148 (2003).

[46] Unwin, S.C. & Shao, M. Space Interferometry Mission. in *Interferometry in Optical Astronomy* (eds. P. J. Lena & A. Quirrenbach) 754-761 (2000).

[47] Perryman, M.A.C. GAIA Spectroscopy: Science and Technology. in ASP Conference Proceedings, Vol. 298 (ed. Ulisse Munari) p. 3 (ASP Conf. Series, 2003).

[48] Arnold, I. & Schneider, J. The detectability of extrasolar planet surroundings I. Reflected-light photometry of unresolved rings. astro-ph/0403330 (2004).

[49] Mather, J.C. and Stockman, H.S. *Proc. SPIE* **4013**, 2-16 (2000).

[50] Akeson, R.L., Swain, M. R., & Colavita, M.M. Differential phase technique with the Keck Interferometer. in *Interferometry in Optical Astronomy* (ed. P. J. Lena) *Proc. SPIE* **4006**, 321-327 (2000).

[51] Akeson, R.L. & Swain, M.R. Differential Phase Observations of Extrasolar Planets with the Keck Interferometer. in *From Giant Planets to Cool Stars*, (ed. C.A. Griffith & M.S. Marley) p. 300 (ASP Conference Series Vol. 212, 2000)

[52] Paresce, F. Scientific Objectives of the VLTI Interferometer. *The Messenger* **104**, 5-7 (2001).

[53] Beuzit, J.-L., et al. The Planet Finder project for the VLT. in *SF2A-2004: Semaine de l'Astrophysique Francaise* (eds. F. Combes, D. Barret, T. Contini, F. Meynadier & L. Paganii) p. 32 (EdP-Sciences, Conference Series, 2004).

[54] Macintosh, B. et al. Extreme Adaptive Optics Planet Imager (XAOPI). in *Techniques and Instrumentation for Detection of Exoplanets.* (ed. Coulter, D. R.) pp. 272-282 (Pro-

ceedings of the SPIE, Vol. 5170, 2003).

[55] Tamura, Itoh, I., & Oasa, Y. Searches for Extrasolar Planets with the Subaru Telescope: Companions and Free-Floaters. in *Proceedings of the IAU 8th Asian-Pacific Regional Meeting: Volume I*, (ed. Satoru Ikeuchi, John Hearnshaw and Tomoyuki Hanawa) pp. 73-76 (San Francisco, Astronomical Society of the Pacific, Vol. 289, 2003).

[56] Hinz, P.M., Angel, J.R.P., Woolf, N.J., Hoffman, W.F., & McCarthy, D.W. BLINC: a testbed for nulling interferometry in the thermal infrared. in *Interferometry in Optical Astronomy* (ed. P.J. Lena) *Proc. SPIE* **4006**, 349 (2000).

[57] Hinz, P.M. Nulling interferometry for studying other planetary systems: Techniques and observations. PhD Thesis, The University of Arizona (2001).

[58] Hawarden, T.G., Gilmozzi, R., & Hainaut, O. Using a 100-meter ELT (e.g., "OWL") for Extrasolar Planet and Extrasolar Life Detection. in *Scientific Frontiers in Research on Extrasolar Planets* ASP Conference Series, Vol. 294 (ed. Drake Deming and Sara Seager) pp. 581-586 (San Francisco: ASP, 2003).

[59] Davison, W.B., Woolf, N.J., & Angel, J.R.P. Design and Analysis of 20-m track mounted and 30-m telescopes. in *Future Giant Telescopes* (eds. Angel, J.R.P. & Gilmozzi, R.) Proceedings of the SPIE, Vol. 4840, pp. 533-540 (2003).

[60] Strom, S. Toward a Giant Segmented Mirror Telescope: A Progress Report from AURA's New Initiatives Office. American Astronomical Society Meeting 203, # 24.04 (2003).

[61] Aristidi, E., Agabi, A., Vernin, J., Azouit, M., Martin, F., Ziad, A., & Fossat, E. Antarctic site testing: First daytime seeing monitoring at Dome C. *Astron. Astrophys.* **406**, L19-L22 (2003).

[62] Schneider, G. et al. Domains of observability in the near-infrared with HST/NICMOS and adaptive-optics augmented large ground-based telescopes. unpublished manuscript

at http://nicmosis.as.arizona.edu:8000/REPORTS/NICMOS_AO_WHITEPAPER.html (2002).

[63] Shao, M., Levine, B.M., Wallace, J.K., Serabyn, E., & Liu, D.T. The Visible Nulling Coronagraph–Progress Towards Mission and Technology Development. *BAAS* **203**, #03.04 (2003).

[64] Trauger, J. et al. Eclipse, A Direct Imaging Investigation of Nearby Planetary Systems. *BAAS* **197**, # 49.07, p. 1486 (2000).

[65] Trauger, J., Hull, A.B., & Redding, D.A. Eclipse Test Bed for Very High Contrast Space Astronomy. *BAAS* **199**, # 86.04 p. 1431 (2001).

[66] Beichman, C.A., Coulter, D.R., Lindensmith, C., & Lawson, P.R. Selected Mission Architectures For The Terrestrial Planet Finder (TPF): Large, Medium, and Small. in *Future Research Direction and Visions for Astronomy.* (ed. Dressler, Alan M.), Proceedings of the SPIE, Vol. 4835, pp. 115-121 (2002).

[67] Matthews, J.M., Kuschnig, R., & Shkolnik, E. Ultraprecise photometry from space: exploring pulsations with the "Humble Space Telescope." in *Proceedings of the SOHO 10/GONG 2000 Workshop: Helio- and asteroseismology at the dawn of the millennium* (ed. A. Wilson) ESA SP-464, Noordwijk: ESA Publications Division, pp. 385-390 (2001).

[68] Roadmap for the Office of Science *Origins* theme. NASA/JPL-400-1060 (2003); NASA 2003 Strategic Plan. Document # NP-2003-01-298-HQ (2003).

[69] Keats, J. On First Looking into Chapman's Homer. (1816).

[70] Racine, R., Walker, G.A.H., Nadeau, D., Doyon, R. & Marois, C. Speckle Noise and the Detection of Faint Companions. *Publications of the Astronomical Society of the Pacific* **111**, 587-594 (1999).

Correspondence and requests for materials should be addressed to Adam Burrows (bur-

rows@as.arizona.edu).

The author acknowledges David Sudarsky, Ivan Hubeny, Bill Hubbard, Jonathan Lunine, Jim Liebert, Jason Young, John Trauger, Jonathan Fortney, Aigen Li, Christopher Sharp, and Drew Milsom for fruitful conversations or technical aid and help during the course of this work, as well as NASA and the NASA Astrobiology Institute for their financial support.

TABLES

TABLE I. Interesting EGPs Listed by Angular Separation

EGP	$a(1+e)/d$ $(")^a$	star	a (AU)	d (pc)	P	$M_p \sin(i)$ (M_J)	e
ϵ Eri b	1.61	K2V	3.3	3.2	6.85 yrs.	0.86	0.61
55 Cnc d	0.51	G8V	5.9	13.4	14.7	4.05	0.16
47 UMa c	0.31	G0V	3.73	13.3	7.10	0.76	0.1
HD 160691c	0.27	G3IV-V	2.3	15.3	3.56	$\sim$1	$\sim$0.8
υ And d	0.27	F8V	2.50	13.5	3.47	4.61	0.41
HD 39091b	0.26	G1IV	3.34	20.6	5.70	10.3	0.62
Gl 777A b	0.23	G6V	3.65	15.9	7.15	1.15	$\sim$0
14 Her b	0.20	K0V	2.5	17	4.51	3.3	0.33
47 UMa b	0.17	G0V	2.09	13.3	2.98	2.54	0.06
HD 33636b	0.17	G0V	3.56	28.7	4.43	7.71	0.41
HD 10647b	0.16	F9V	2.10	17.3	2.89	1.17	0.32
γ Cephei b	0.15	K2V	1.8	11.8	2.5	1.25	$\sim$0
HD 147513b	0.15	G3V	1.26	12.9	1.48	1.0	0.52
HD 216437b	0.134	G4V	2.7	26.5	3.54	2.1	0.34
HD 160691b	0.127	G3IV-V	1.48	15.3	1.74	1.7	0.31
HD 70642b	0.121	G5IV-V	3.3	29	4.79	2.0	0.10
HD 50554b	0.109	F8V	2.38	31.03	3.50	4.9	0.42
HD 106252b	0.108	G0V	2.61	37.44	4.11	6.81	0.54
HD 168443c	0.107	G5V	2.87	33	4.76	17.1	0.23
HD 10697b	0.075	G5IV	2.0	30	2.99	6.59	0.12
υ And c	0.072	F8V	0.83	13.5	241 days	2.11	0.18
GJ 876b	0.049	M4V	0.21	4.72	61.0	1.89	0.1
GJ 876c	0.036	M4V	0.13	4.72	30.1	0.56	0.27

HD 114762b	0.017	F9V	0.35	28	84.0	11.0	0.34
55 Cnc b	8.4×10^{-3}	G8V	0.12	13.4	14.7	0.84	0.02
υ And b	4.5×10^{-3}	F8V	0.059	13.5	4.62	0.71	0.034
51 Peg b	3.4×10^{-3}	G2V	0.05	14.7	4.23	0.44	0.01
τ Boo b	3.3×10^{-3}	F7V	0.05	15	3.31	4.09	$\sim$0
HD 49674b	1.6×10^{-3}	G5V	0.057	40.7	4.95	0.12	0.17
HD 209458b	9.6×10^{-4}	G0V	0.045	47	3.52	0.69	$\sim$0
HD 83443b	9.4×10^{-4}	K0V	0.038	43.5	2.99	0.35	0.08
OGLE-TR56b	1.5×10^{-5}	G0V	0.023	$\sim$1500	1.21	1.45	$\sim$0

[a] Maximum possible angular separation (at apoapse/apastron).

Figure 1. Profiles of atmospheric temperature (in Kelvin) versus the logarithm base ten of the pressure (in bars) for a family of irradiated 1-M_J EGPs around a G2V star as a function of orbital distance. Note that the pressure is decreasing along the ordinate, which thereby resembles altitude. The orbits are assumed to be circular, the planets are assumed to have a radius of 1 R_J, and the orbital separations vary from 0.2 AU to 15 AU. The intercepts with the dashed lines identified with either $\{NH_3\}$ or $\{H_2O\}$ denote the positions where the corresponding clouds form. Taken from Burrows, Sudarsky, and Hubeny [33]. See text for a discussion.

Figure 2. Planet to star flux ratios versus wavelength (in microns) from 0.5 μm to 30 μm for a 1-M_J EGP with an age of 5 Gyr orbiting a G2V main sequence star similar to the Sun. This figure portrays ratio spectra as a function of orbital distance from 0.2 AU to 15 AU. Zero eccentricity has been assumed and the planet spectra have been phase-averaged as described in Sudarsky, Burrows, and Hubeny [45]. The associated T/P profiles are given in Fig. 1. Note that the planet/star flux ratio is most favorable in the mid-infrared. Water features at 0.94 μm, 1.2 μm, 1.4 μm, 1.9 μm, 2.6 μm, and 6.5–8 μm, methane features in the optical and at 0.89 μm, 2.2 μm, 3.3 μm, and 7.8 μm, carbon monoxide features at 2.3 μm and 4.67 μm, the Na-D doublet at 0.589 μm, and the K I doublet at 0.77 μm help shape these spectra. Taken from Burrows, Sudarsky, and Hubeny [33]. See text for discussion.

Figure 3. The logarithm of the absolute flux in milliJanskays ($\equiv 10^{-26}$ ergs cm^{-2} s^{-1} Hz^{-1}) at 10 parsecs for a "Class V" roaster versus wavelength (in microns) from 0.4 μm to 5 μm. This could be a 1-M_J EGP in a 0.05 AU orbit around a solar-type star. The planet spectrum has been phase-averaged as described in Sudarsky et al. [39,45]. Shown are the positions of various relevant molecular bands and atomic lines. Figure taken from Sudarsky, Burrows, & Hubeny [45]. See text for discussion.

Figure 4. Keplerian orbital elements. The intersection of the orbit plane with the observational plane defines the angles i, ω, Ω, and θ. The angle between the observer (Earth) and the line of nodes (intersection of the orbit plane with the horizontal plane) is the longitude of the ascending node (Ω), the angle between the line of nodes and the focus(star,

in yellow)–periapse(black dot) is the argument of periastron (ω), the angle between the orbit plane and the Z-axis (perpendicular to the horizontal plane) is the inclination (i), and the angle between the focus–periapse line and the position of the planet (red dot) is the true anomaly (θ). See text for details.

Figure 5. A comparison of the planet/star contrast ratios (and contrast magnitudes $= -2.5\log(f)$) versus angular separation (in arcseconds) achievable for some proposed planet imaging systems. A distance of 10 parsecs is assumed. Integration times and signals-to-noise assumed vary and are taken from preliminary studies by the associated instrument teams. At H band (red), the imaging telescopes represented include the Canada/France/Hawaii Telescope (CFHT) [70], HST/NICMOS, and the Gemini/XAOPI. Not shown on this plot is the MMT (AO) system, which should achieve at a wavelength of 5 μm fs from 10^{-4} to a few $\times 10^{-6}$ for angular separations of $0.3''$ to $1.0''$, respectively. The LBT, also not shown, should achieve at a wavelength of 10 μm approximately $10\times$ better performance than this. At 5 μm , a notional curve for a 20- or 30-meter telescope in Antarctica and the JWST (in fact at 4.6 μm) are provided. At 10 μm , a notional curve for a 100-meter in Antarctica is given. Also included on this plot is the interferometric version of TPF (TPF-I/Darwin), which might have a sensitivity of one part in 10^7 from 5 μm to 20 μm . All the mid-infrared curves are in blue. In the optical (green, V), putative sensitivities for *EPIC*, *ECLIPSE*, and TPF-C are plotted. Superposed are corresponding "phase-averaged" theoretical curves (dashed) for a 5-Gyr/1-M_J EGP around a G2V star in the H band ($\sim$1.65 μm), in the 4–5 μm band, and at 10 μm (see Fig. 2). Also included are a theoretical curve in the H band (dashed red) for a 0.5-Gyr/7-M_J EGP around a G2V star and a green swathe where the known EGPs may reside in the optical (V band). Note that the theoretical curves for more massive and younger EGPs than represented on this plot can be *considerably* higher. Orientation effects have been ignored. Each curve is for a given wavelength or bandpass and the imager and theory must be compared at the same wavelength. Very generous error bars should be assumed. The photometric sensitivity curves for MOST and *Kepler* are also superposed. See text for details.

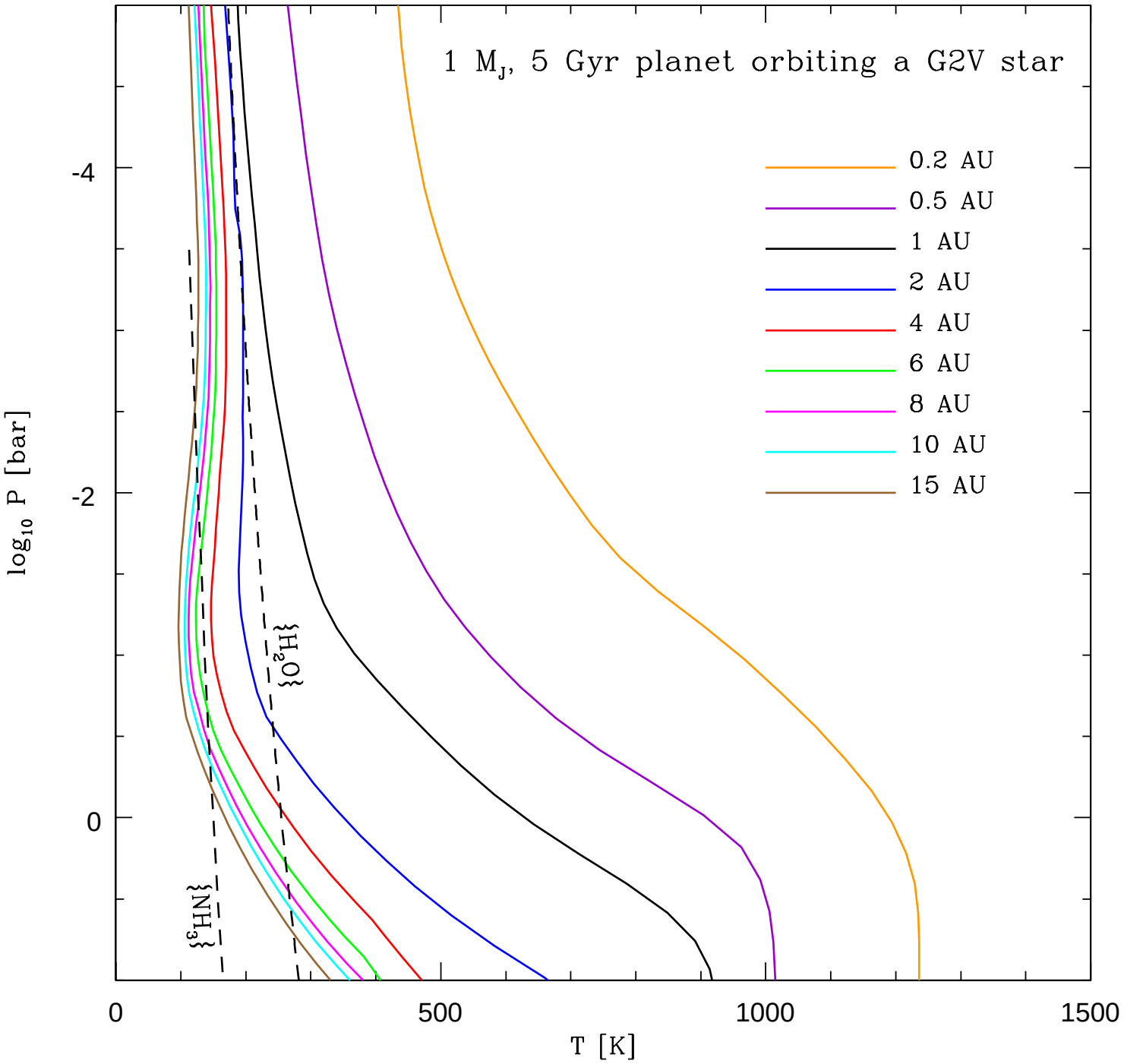
1 M$_J$, 5 Gyr planet orbiting a G2V star
0.2 AU
0.5 AU
1 AU
2 AU
4 AU
6 AU
8 AU
10 AU
15 AU
{H$_2$O}
{NH$_3$}
log$_{10}$ P [bar]
-4
-2
0
0
500
1000
1500
T [K]

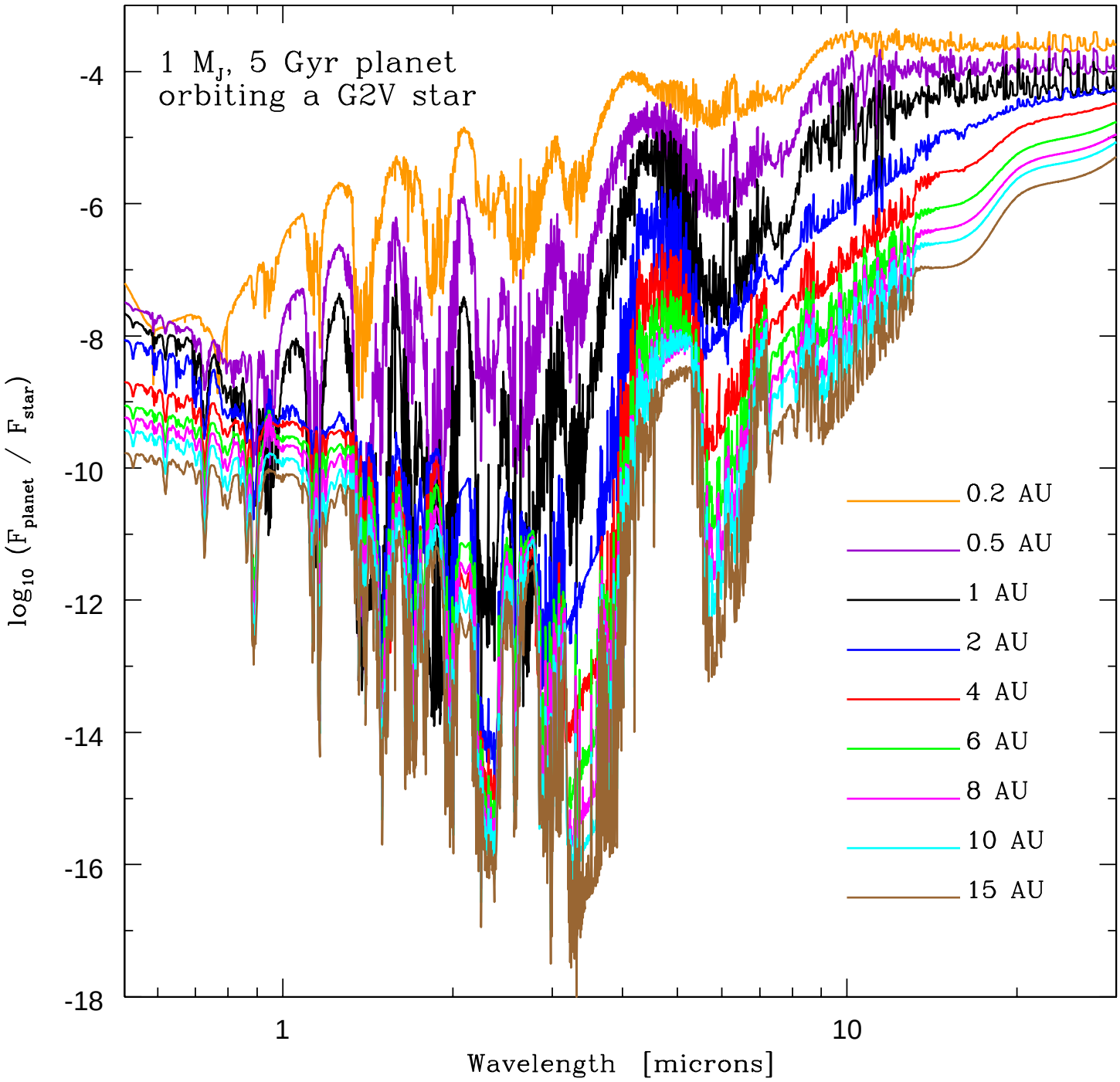
1 M$_J$, 5 Gyr planet
orbiting a G2V star
-4
-6
-8
-10
-12
-14
-16
-18
log$_{10}$ (F$_{planet}$ / F$_{star}$)
1
10
Wavelength [microns]
0.2 AU
0.5 AU
1 AU
2 AU
4 AU
6 AU
8 AU
10 AU
15 AU

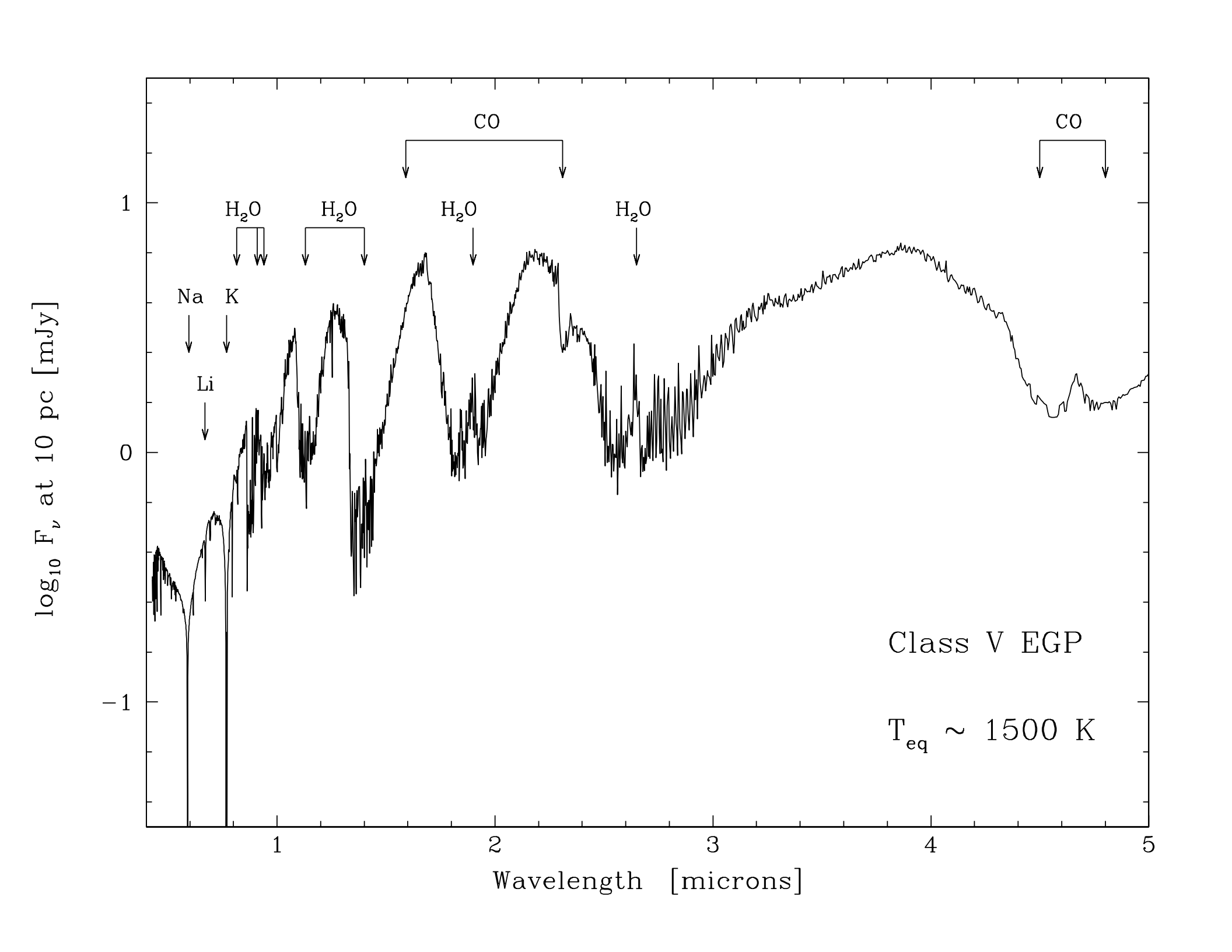
CO
CO
H2O
H2O
H2O
H2O
Na
K
Li
Class V EGP
Teq ~ 1500 K
log10 Fν at 10 pc [mJy]
Wavelength [microns]
1
0
−1
1
2
3
4
5

This figure "figure5.jpg" is available in "jpg" format from:

http://arXiv.org/ps/astro-ph/0501484v1